Bulletin of the Seismological Society of America, Vol. 101, No. 1, pp. 438–445, February 2011, doi: 10.1785/0120100074

*Short Note*

# The 8 June 2008 $M_w$ 6.4 Earthquake in Northwest Peloponnese, Western Greece: A Case of Fault Reactivation in an Overpressured Lower Crust?

by K. I. Konstantinou, C. P. Evangelidis, and N. S. Melis

**Abstract** On 8 June 2008 a strong ($M_w$ 6.4) earthquake occurred in the area of northwest Peloponnese, western Greece. The event originated in the lower crust and was caused by the rupture of a previously unknown fault probably inherited from past tectonic phases. In this study we perform a stress inversion of all available focal mechanisms in this area in order to obtain an estimate of the regional stress field. It is shown that the maximum principal stress axis has an azimuth of N273°E and forms an angle of 63° with the fault's strike, which is well-constrained by seismological observations. This implies that the fault was severely misoriented with respect to the prevailing stress field assuming friction coefficients in the range 0.65–0.85. Calculation of pore-fluid factors for a variety of input parameters seems to confirm the presence of elevated fluid pressure near the hypocenter because they reach superhydrostatic to lithostatic values (0.80–1.0). The source of these fluids is probably of deep origin and may have to do with upper mantle degassing. This suggestion is supported by the presence of mantle helium in spring waters close to the epicenter and by low *Pn* velocities consistent with partially molten mantle beneath northwest Peloponnese.

*Online Material:* Moment-tensor solutions used in the stress inversion and tomographic velocity variations and helium isotopes measurements.

## Introduction

From the viewpoint of seismologists, the term "fault reactivation" can be defined as the occurrence of an earthquake along a preexisting fault (Collettini *et al.*, 2005). This process is mechanically easier than forming a new fault and is dependent on the frictional conditions within the fault zone. Fault structures that are inherited from previous tectonic processes (such as orogeny) are likely candidates for reactivation because it has been found that they are responsible for much of the localized deformation within the continental lithosphere (Butler *et al.*, 2006). Moreover, the fact that such faults rarely have a surface expression and the interseismic period from one seismic event to the next is usually unknown, makes them particularly dangerous in terms of seismic hazard. Typical reactivation examples of such deep, inherited faults described in the literature include the 1990–1991 Potenza (Di Luccio, Piscini, *et al.*, 2005; Boncio *et al.*, 2007) and 2002 Molise earthquakes (Di Luccio, Fukuyama, Pino, 2005).

Western Greece is an area that is characterized by complicated tectonics and the frequent occurrence of moderate to large earthquakes. Two geodynamic processes are responsible for this activity, namely continent–continent collision in the north and ocean–continent subduction along the Hellenic trench in the south (Baker *et al.*, 1997; Sachpazi *et al.*, 2000; Laigle *et al.*, 2002; Fig. 1a). The dextral strike-slip Kefalonia transform fault (KTF) marks the transition between these two regimes and has generated several large events in the past, the most recent being the 2003 ($M_w$ 6.3) Lefkada earthquake. The Alpine collision affected northwest Peloponnese during the Eocene and resulted in the formation of the Hellenic mountain range and the development of thrust faulting in the area (Kamberis *et al.*, 2000 and references therein). Since the early Pliocene until present postcompressional normal faulting has prevailed, generating a number of basins that were filled initially with marine and later with terrestrial fluvial deposits.

Catalogs of historical earthquakes indicate a low seismicity potential for northwest Peloponnese, because only one large event in 1806 is believed to have originated near there

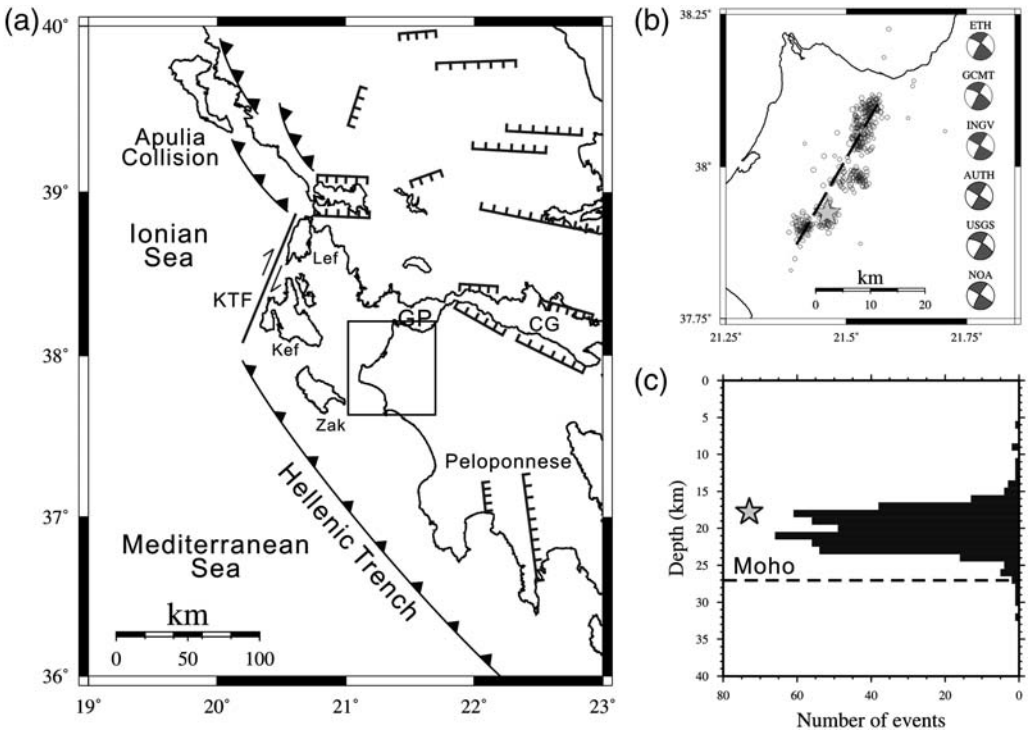


**Figure 1.** (a) Map showing the tectonic setting in western Greece. Major faults and plate boundaries have been adopted from Papazachos and Papazachou (1997). KTF: Kefalonia Transformation Fault, Kef: Kefalonia island, Lef: Lefkada island, Zak: Zakynthos island, GP: Gulf of Patras, CG: Gulf of Corinth; (b) expanded view of the area inside the square shown in (a). Open circles represent aftershock epicenters of the 8 June earthquake and the star is the mainshock (after Konstantinou *et al.*, 2009). The thick dashed line indicates the strike of the fault taken from the moment tensor solutions that are shown at the right hand side of the plot. ETH: Swiss Seismological Service, GCMT: Global CMT solution, INGV: Italian Institute of Geophysics and Volcanology, AUTH: Aristotle University of Thessaloniki, USGS: United States Geological Survey, NOA: National Observatory of Athens; (c) depth-frequency distribution of all aftershocks shown in (b). Also shown is the depth of the mainshock as a star and the depth of the Moho found by receiver function studies.

(Papazachos and Papazachou, 1997). However, on 8 June 2008 a strong earthquake with a moment magnitude of 6.4 occurred in the same area causing two casualties, extensive damage to buidlings and bending of rail lines (Kalogeras *et al.*, 2008). The event was considered unusual in the sense that first hypocentral estimates pointed to a relatively deep source ($>15$ km), and it occurred in an area where no previous seismological or other observations suggested the existence of a seismogenic fault at such depths. Konstantinou *et al.* (2009) performed a detailed analysis of all the available regional waveform data for this seismic sequence collected by the National Observatory of Athens (NOA). Using waveform cross-correlation methods the mainshock was accurately relocated at a depth of 18 km, and 438 of its aftershocks formed three distinct clusters at 15–25 km depths (Fig. 1b,c). Horizontal and vertical errors associated with these locations did not exceed 1 km (see Konstantinou *et al.*, 2009). The moment tensor solution inferred from inversion of regional waveforms showed a purely strike-slip mechanism and was very similar with solutions published by other agencies. The fault's strike, as determined by seismological means, is N210°E and agrees well with the direction of the relocated aftershock clusters. Recent estimates of the Moho depth in the Greek region using receiver functions (Sodoudi *et al.*, 2006) suggest that the Moho in northwest Peloponnese lies at about 27 km, placing the focus of the mainshock in the lower crust.

These observations were interpreted by Konstantinou *et al.* (2009) as indications of the reactivation of a fault that was inherited from past tectonic processes that affected northwest Peloponnese. An important condition for reactivation to occur is that the seismogenic fault is favorably oriented with respect to the direction of $\sigma_1$ stress axis; otherwise it is considered unfavorably oriented or even severely misoriented (Sibson, 1990). This article investigates the relationship between the regional stress field in northwest Peloponnese and the orientation of the fault that generated the 8 June event. We first determine the regional stress field in the study area by means of a stress inversion of available focal mechanisms. Then we consider the fault's orientation inside this stress field and provide evidence that the reactivated fault was severely misoriented and its failure was assisted by elevated fluid pressure near the hypocenter. The likely deep origin of these fluids is finally discussed along with the significance of these findings for seismic hazard evaluation in western Greece.

## Regional Stress Field

Stress inversion of earthquake focal mechanisms is the most usual way to determine the regional stress field in an area. There is only a small number of available teleseismic moment tensor solutions for northwest Peloponnese that mostly correspond to moderate size earthquakes. For the purpose of obtaining a larger number of focal mechanisms, we first searched the catalog of NOA for events that occurred in this area that are large enough ($M_L > 3.5$) in order to derive moment tensor solutions by regional waveform inversion. We use data recorded by HL, which is the permanent seismic network maintained by NOA consisting of 23 three-component broadband seismometers that cover most parts of Greece and has been operating in digital mode since 2000 (see the Data and Resources section). A linear, time-domain moment tensor inversion method with a point-source approximation is applied to model the three-component waveforms of these events. The quality of the resulting solution is assessed by considering the average waveform misfit (quality range *A*–*D*, with *A* indicating a unit normalized misfit lower than 0.3 and *D* indicating larger than 0.7) and the percentage of the non-double-couple part of the solution (quality range 1–4, with 1 indicating a percentage smaller than 20% and 4 indicating larger than 80%). The application of this method to events in the Greek region is described in great detail in Konstantinou *et al.* (2010) to which the interested reader is referred for more information. In this way, we obtained 17 additional moment tensor solutions determined from NOA data where most of them are of quality *A* or *B*. Additionally, we found one more event of quality *A* in the regional CMT (RCMT) moment tensor database and one event in the database of the Swiss Seismological Service provided by Eidgenössische Technische Hochschule Institute in Zurich (see the Data and Resources section). Finally, we searched the Global CMT (GCMT) database in order to find well-constrained solutions that pass the criteria set by Frohlich and Davis (1999). These criteria specify that (1) the square root of the ratio of the sum of standard error elements to the sum of the corresponding moment tensor elements should be less than 0.15; (2) the non-double-couple part of the solution is less than 40%; and (3) no moment tensor element is fixed during the inversion. Only two GCMT solutions in northwest Peloponnese were consistent with these criteria. Ⓔ Table S1 in the electronic supplement to this paper lists the source parameters of the 21 focal mechanisms that were used for stress inversion; Figure 2 shows the focal mechanism plots in map view and the inversion results. It should be noted that none of the included events corresponds to aftershocks of the 8 June earthquake or any other earthquake in this area. This ensures that the inversion results are not biased by a nonrandom distribution of focal mechanisms.

A linear least-squares inversion method proposed by Michael (1987) is utilized in order to find the best-fitting stress tensor that corresponds to our dataset of nodal planes. The method is based on two assumptions, namely that earthquakes slip in the direction of the resolved shear stress on the fault plane and that the stress field can be considered homogeneous over the space/time scale covered by the dataset. The stress tensor is expressed in terms of the orientation of the three principal stress axes ($\sigma_1$, $\sigma_2$, $\sigma_3$) and the parameter $R$ given by

$$R = \sigma_2 - \sigma_3/\sigma_1 - \sigma_3, \quad (1)$$

which indicates the relative magnitudes of the stress axes. Confidence regions are estimated using a bootstrap technique, where the dataset is resampled with replacement

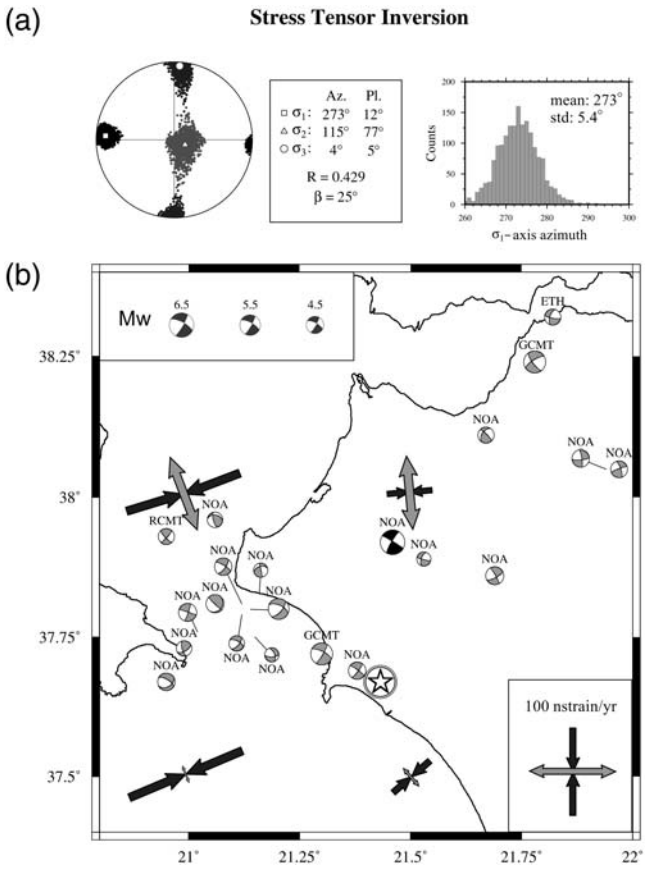


**Figure 2.** (a) Lower hemisphere projection of the directions of principal stress axes obtained from inversion of focal mechanisms. The dots define the 95% confidence region of each stress axis (Az: Azimuth, Pl: Plunge in degrees, $R$ is given in equation 1, and $\beta$ is the average misfit between the best-fit model and the data). Also shown is a histogram representing the distribution of the $\sigma_1$ axis azimuth for the samples surrounding the best-fit estimate. (b) Available focal mechanism solutions for the area of northwest Peloponnese. Gray focal mechanism plots indicate solutions derived from waveform inversion of NOA data, or taken from the GCMT, RCMT and ETH databases (see text for more details). Superimposed on this plot are the principal strain axes derived from GPS data taken from Hollenstein *et al.* (2008). The black beach ball indicates the focal mechanism of the 8 June main event. The star inside the circle represents the location of helium measurement taken from Pik and Marty (2009) (see the Discussion and Conclusions section).

hundreds or thousands of times. In this paper we use 2000 bootstrap resamplings that are adequate to produce stable confidence regions up to the 95% level (Michael, 1987; Hardebeck and Hauksson, 2001). The average misfit $\beta$ between the best-fit model and the data is also calculated and is utilized in order to infer whether the stress field can be considered as homogeneous or not. Hardebeck and Hauksson (2001) have shown using synthetic data that this method provides robust confidence regions and can work well even with noisy datasets. Figure 2 shows the results of this method when applied to the available 21 focal mechanisms obtained previously. It can be seen that the maximum stress axis $\sigma_1$ has an azimuth of N273°E and is subhorizontal, while minimum stress axis $\sigma_3$ lies at an azimuth of N4°E in good agreement with the GPS-derived principal strain axes in northwest Peloponnese published by Hollenstein *et al.* (2008). The average misfit is of the order of 25° indicating a good fit if we assume fault plane solution errors between 10° and 20° (Michael, 1991). The distribution of the azimuth values for the $\sigma_1$ axis determined for each bootstrap resampling contained in the confidence area shown in Figure 2 exhibits a mean value of 273° and a standard deviation $\sigma = 5.4°$, implying an uncertainty of 11° ($= 2\sigma$) at a 95% confidence level.

## Fault Orientation and Reactivation

Sibson (1990) derived an expression that described the relative ease of reactivation of preexisting faults with varying orientations in the prevailing stress field. This expression is given by

$$Q = (\sigma_1 - P_f)/(\sigma_3 - P_f) = (1 + \mu_s \cot\theta)/(1 - \mu_s \tan\theta), \quad (2)$$

where $P_f$ is the fluid pressure within the rock mass, $\mu_s$ is the static coefficient of rock friction, and $\theta$ is the reactivation angle between the fault plane and the maximum stress axis. Assuming typical values of rock friction ($\mu_s = 0.65$–$0.85$), the stress ratio $Q$ needed to reactivate a preexisting fault can be seen as a function of the reactivation angle $\theta$ (Fig. 3). Each diagram is divided in three domains according to the value range of $\theta$: favorably oriented, unfavorably oriented, and severely misoriented. The optimal angle for favorable orientation is equal to $0.5 \arctan(1/\mu_s)$; in the case of the lowest friction coefficient, it is about 28°. In this case the fault remains favorably oriented even when the reactivation angle departs from the optimal by ±15° (Sibson, 1990). After that point the stress ratio required for reshear increases steadily, and faults are considered unfavorably oriented. When the reactivation angle assumes a value that is larger than twice the optimal value ($= 56°$ for $\mu_s = 0.65$), faults become severely misoriented. Similar considerations apply for larger friction coefficients as shown in Figure 3. A necessary prefailure condition for unfavorably or severely misoriented faults is

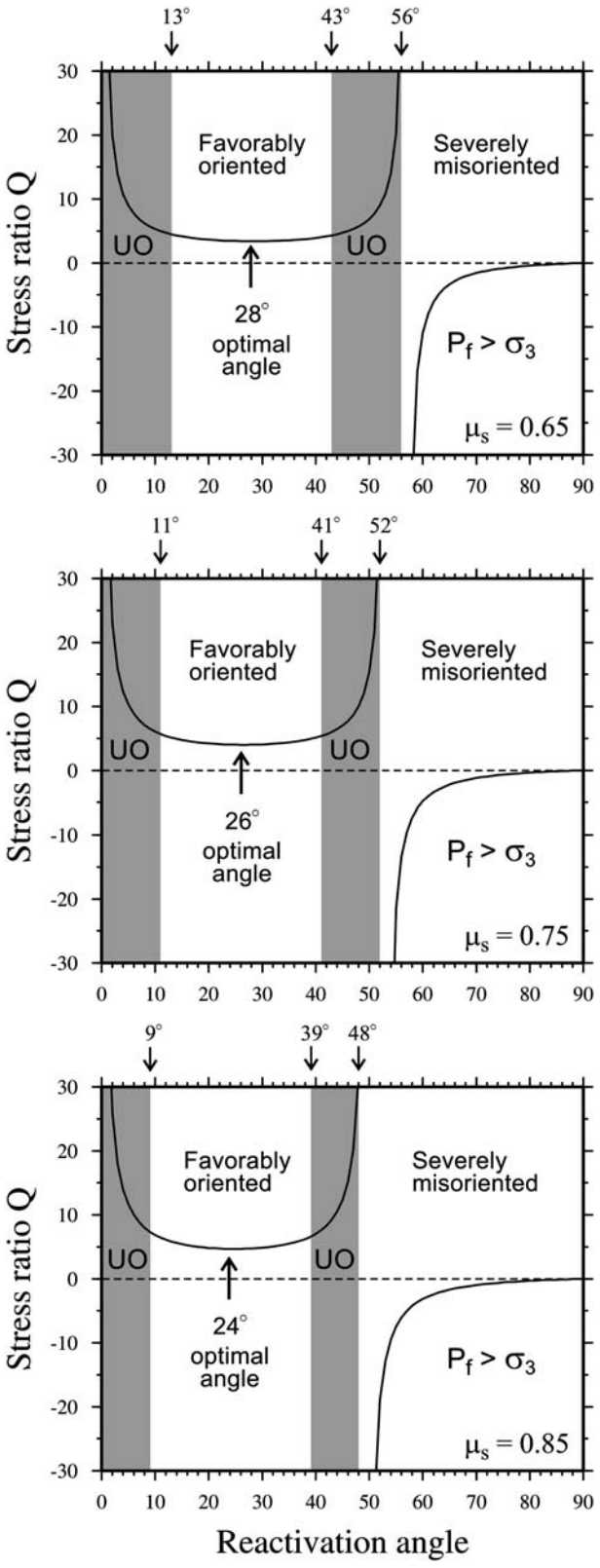


**Figure 3.** Diagrams showing the variation of stress ratio $Q$ as a function of reactivation angle for three different values of static friction coefficient (after Sibson, 1990). Gray shaded areas define the domains that the fault becomes Unfavorably Oriented (UO) starting at 15° of the optimal angle for reactivation and becoming severely misoriented for angles that are twice the optimal value.

that $P_f > \sigma_3$, implying high pore-fluid pressure within the fault zone.

The fault that generated the 8 June earthquake exhibits a strike that is about N210°E showing a variation of only 1°–3° among the solutions reported by several agencies (see Fig. 1b and Konstantinou *et al.*, 2009). Based on this strike and the mean azimuth of the $\sigma_1$ axis (273°), we infer that the reactivation angle is equal to 63°, indicating that the fault is severely misoriented. We also consider how this angle will change if we take into account the uncertainty of the $\sigma_1$ axis azimuth that can be quantified as twice the standard deviation determined earlier (~11°). In this case, the smallest value of $\theta$ will be 52°, where based on the diagram corresponding to the lowest friction coefficient the fault is still considered as unfavorably oriented, requiring elevated pore-fluid pressure to reach failure.

An alternative explanation for the reactivation of a misoriented fault is that the fault zone may consist of inherently weak material (friction coefficient much less than 0.6) that would extend the domain of favorable orientation to larger $\theta$ values without having to invoke the presence of fluids. However, most fault gouge minerals that exhibit such a weak behavior at shallow depths are found to be significantly stronger at larger depths (> 10 km) based on laboratory experiments (Morrow *et al.*, 2000 and references therein). For example, chrysotile, a fault gouge mineral, exhibits a friction coefficient of 0.3–0.4 up to 6 km depth, which is increasing to 0.55–0.7 at 10 km (Tembe *et al.*, 2009). Talc may be an exception to this trend because it remains weak ($\mu < 0.2$) for a considerable depth range. Although talc could be a fault gouge mineral, the problem with such a suggestion is that talc is more likely to lead to stable fault creep rather than seismogenic behavior. Therefore, the large nucleation depth of the 8 June earthquake suggests that the observed fault misorientation cannot be explained by the presence of weak material.

## Calculation of Pore-Fluid Factors

Streit and Cox (2001) investigated fluid pressure conditions for the reactivation of misoriented faults by determining pore-fluid factors $\lambda = P_f/\rho g z$ (where $\rho$ is rock density, $g$ is acceleration of gravity, and $z$ is depth). The authors considered a fault that maintains some cohesiveness, has an internal friction coefficient $\mu_f$, and is surrounded by intact rock. Assuming that the effective overburden pressure is equal to the intermediate principal stress axis and using two-dimensional failure criteria, they derived the pore-fluid factor for a strike-slip fault that is given by

$$\lambda = 1 - [-2C + (\sigma_1 - \sigma_3)(\sin 2\theta + \mu_f \cos 2\theta)]/(2\rho g z \mu_f), \quad (3)$$

where $C$ is the cohesive strength of the fault, $(\sigma_1 - \sigma_3)$ is differential stress that drives the fault to failure, and $z$ is the hypocentral depth.

For the case of the 8 June event, the depth is already constrained by previous observations ($z = 18$ km). Local earthquake tomography in northwest Peloponnese indicates that $P$-wave velocity at that depth is 6.5 km/s (Melis and Tselentis, 1998), which is consistent with diabase lithology, therefore $\rho$ is assumed 2962 kg/m$^3$ (see Christensen and Mooney, 1995). Cohesive strength is expected to be larger for deeper faults (e.g., Streit, 1999); also laboratory studies indicate that there is considerable cohesive strengthening (up to 35 MPa) of fault zones experiencing large interseismic periods (Tenthorey and Cox, 2006). Nevertheless, in order to assess its effect on the calculations we treat cohesive strength as a free parameter by selecting two extreme values (0 and 14 MPa). We also use two values of $\theta$ equal to 63° (best-fit estimate) and 52° (best-fit minus the $\sigma_1$ axis uncertainty estimate). Finally, we apply equation (3) for three typical values of friction coefficient ($\mu_f = 0.65$–$0.85$). Figure 4 shows the variation of $\lambda$ as a function of differential stress for different values of cohesive strength, reactivation angle, and friction coefficient. Reasonable values of differential stress that can cause fault failure fall in the range 40–160 MPa as determined from earthquake stress drops and palaeostress estimates obtained from mylonites (Streit and Cox, 2001). Within this range of differential stress the pore-fluid factor attains values in the range 0.80–1.0, implying superhydrostatic to lithostatic fluid pressure near the hypocenter of the 8 June earthquake. Even assuming an uncertainty of 11° in the estimated azimuth of the $\sigma_1$ axis, the fault is still unfavorably oriented with respect to the regional stress field and calculated pore-fluid factors are superhydrostatic (~0.80).

## Discussion and Conclusions

The presence of overpressured fluids within the core of misoriented faults has been found in exhumed fault zones (e.g., Mittempergher *et al.*, 2009) and has long been suggested in order to explain seismicity along misoriented segments of the San Andreas fault (Hardebeck and Hauksson, 1999). The main effect of these fluids is the reorientation of the maximum stress axis within the fractured damage zone of the fault to more favorable angles for reactivation (Rice, 1992; Faulkner *et al.*, 2006). In the case where the fault is nearly vertical and extends to large depths within the lithosphere, it is possible that ascending mantle fluids may be the cause that produces elevated pore-fluid pressure. Several studies (Kennedy *et al.*, 1997; Newell *et al.*, 2005; Kennedy and van Soest, 2007, among others) have investigated the possible mantle contribution to fluids in major fault zones in the western United States, through analyzing helium isotopes distribution in spring water. It was found that locations that exhibited high proportions of mantle-derived $^3$He also coincided with areas of low upper mantle velocities and high shear strain rates. This was interpreted as an indication of a heterogeneous partially molten mantle, its degassing being

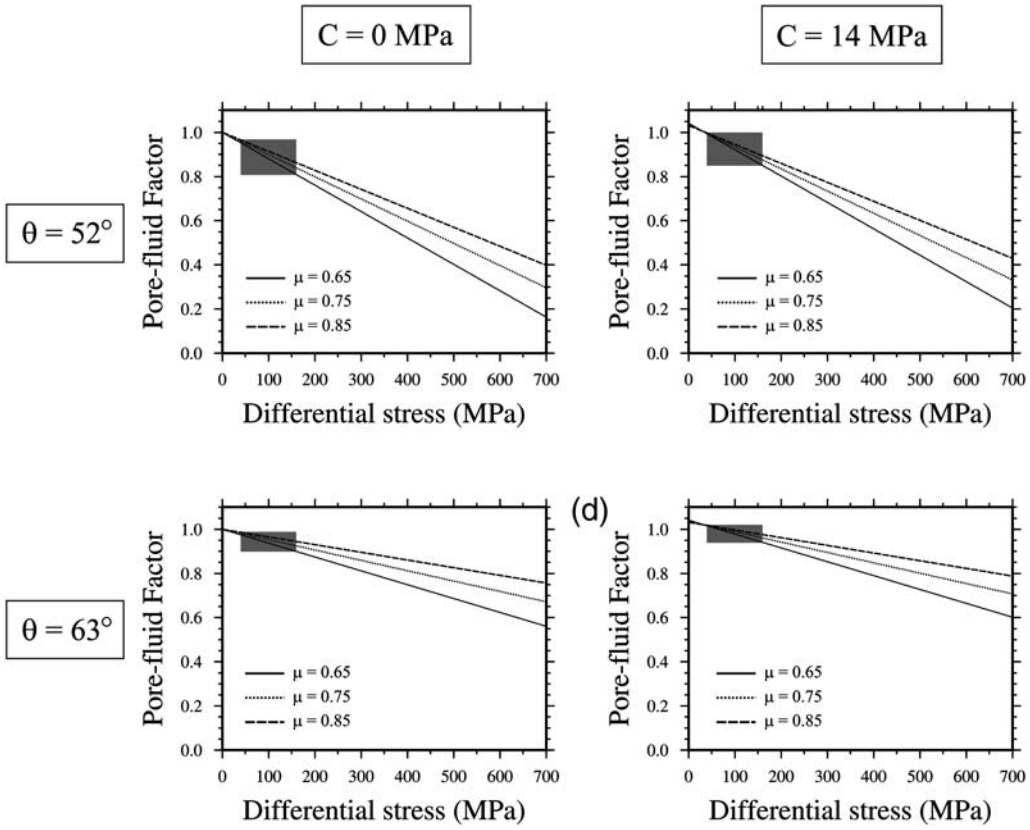


**Figure 4.** Diagram showing the variation of the pore-fluid factor as a function of differential stress for different values of rock friction, cohesive strength and reactivation angles (see text for details). The shaded area signifies differential stress values that can cause the failure of a preexisting fault and their respective pore-fluid factors.

aided by a high degree of deformation in the crust that enhances fault growth and fluid permeability.

Could mantle degassing processes be operating also in northwest Peloponnese resulting in the accumulation of fluids (water and $CO_2$) near the hypocentral area of the 8 June event? In order to answer this question we make use of a database of helium isotope measurements around Greece and surrounding areas recently compiled by Pik and Marty (2009). Indeed, one such measurement taken at a location about 20 km away from the earthquake's epicenter (exact location of the measurement is 37.733° N, 21.383° E shown in Fig. 2) shows a significant percentage (~7%) of mantle helium. Tomographic imaging of *Pn* velocities for the eastern Mediterranean published by Al-Lazki *et al.* (2004) indicate abnormally low values (~7.6 km/s with corresponding errors of the order of 0.055–0.02 km/s) beneath northwest Peloponnese and much of western Greece. These anomalously low *Pn* velocities may represent partially molten areas in the upper mantle that can function as the primary sources of degassing fluids. Furthermore, there is a clear correlation between the locations where mantle helium was detected and areas of low upper mantle velocities (7.6–7.9 km/s) in northern Greece, the Aegean Sea, and western Turkey (Ⓔ see Figure S1 in the electronic supplement to this paper). One could argue that a simple change of the stress boundary conditions in the area could also explain the occurrence of the 8 June event. This suggestion, however, leaves unexplained the misorientation of the fault and overlooks independent observations such as the low *Pn* velocities and the helium isotope measurement close to the epicenter.

In conclusion, our results suggest that the fault that generated the 8 June main event was severely misoriented with respect to the prevailing regional stress field. This means that this strong earthquake probably did not signify the birth of a new fault that would be expected to have a more favorable orientation (Sibson, 1990). Additionally, fluids of deep origin may be responsible for the elevated fluid pressure levels that led to its reactivation. The observations presented here are in agreement with earlier suggestions that deep crustal shear systems may localize the supply of deeply sourced fluids into shallower depths in the seismogenic regime (Cox, 2002). It has to be stressed that such deep, preexisting zones of weakness are likely to exist in other parts of western Greece as well. This adds more complications to the seismic hazard evaluation for this area and calls for a more systematic investigation of its deep structure.

## Data and Resources

The waveform data that were used in this study were recorded by a nationwide network operated by the National

Observatory of Athens. The dataset is not released to the public and it is only available to Greek institutes and their collaborators abroad. The locations of the mainshock and aftershocks of the 8 June earthquake were taken from the electronic supplement accompanying the paper of Konstantinou *et al.* (2009). The Global Centroid Moment Tensor Project database was searched using http://www.globalcmt.org/CMTsearch.html (last accessed March 2010). The Regional Centroid Moment Tensor database was searched using http://www.bo.ingv.it/RCMT/searchRCMT.html (last accessed June 2010). The Swiss Seismological Service Moment Tensor database was searched using http://www.seismo.ethz.ch/prod/tensors/tensors/index_EN(last accessed June 2010). To derive moment tensor solutions by regional waveform inversion, we used data recorded and maintained by NOA found at http://bbnet.gein.noa.gr (last accessed June 2010). Reported moment tensor solutions for the main event were taken from the European-Mediterranean Seismological Centre web page http://www.emsc-csem.org/#2 (last accessed March 2010). The moment tensor solutions were calculated using a software package available at http://eqseis.geosc.psu.edu/~cammon/HTML/MTinvDocs/mtinv01.html (last accessed June 2010). The stress inversion package used is available from http://earthquake.usgs.gov/research/software (last accessed June 2010). Some figures were created using the Generic Mapping Tools (GMT) software package available at http://gmt.soest.hawaii.edu/ (last accessed June 2010).

## Acknowledgments

We would like to thank the National Science Council of Taiwan for the financial support of this research. Thanks are also due to Vasiliki Mouslopoulou for reviewing an earlier version of the paper. Critical comments by two anonymous reviewers and associate editor Cezar Trifu improved the original paper substantially.

## References

Al-Lazki, A. I., E. Sandvol, D. Seber, M. Barazangi, N. Turkelli, and R. Mohamad (2004). *Pn* tomographic imaging of mantle lid velocity and anisotropy at the junction of the Arabian, Eurasian and African plates, *Geophys. J. Int.* **158,** 1024–1040, doi 10.1111/j.1365-246X.2004.02355.x.

Baker, C., D. Hatzfeld, H. Lyon-Caen, E. Papadimitriou, and A. Rigo (1997). Earthquake mechanisms of the Adriatic Sea and western Greece: Implications for the oceanic subduction-continental collision transition, *Geophys. J. Int.* **131,** 559–594.

Boncio, P., T. Mancini, G. Lavecchia, and G. Selvaggi (2007). Seismotectonics of strike-slip earthquakes within the deep crust of southern Italy: Geometry, kinematics, stress field and crustal rheology of the Potenza 1990–1991 seismic sequences ($M_{max}$ 5.7), *Tectonophysics* **445,** 281–300, doi 10.1016/j.tecto.2007.08.016.

Butler, R. W. H., E. Tavarnelli, and M. Grasso (2006). Structural inheritance in mountain belts: An Alpine–Apennine perspective, *J. Struct. Geol.* **28,** 1893–1908, doi 10.1016/j.jsg.2006.09.006.

Christensen, N. I., and W. D. Mooney (1995). Seismic velocity structure and composition of the continental crust: A global view, *J. Geophys. Res.* **100,** 9761–9788.

Collettini, C., L. Chiaraluce, S. Pucci, M. R. Barchi, and M. Cocco (2005). Looking at fault reactivation matching structural geology and seismological data, *J. Struct. Geol.* **27,** 937–942, doi 10.1016/j.jsg.2004.10.016.

Cox, S. F. (2002). Fluid flow in mid- to deep crustal shear systems: Experimental constrains, observations on exhumed high fluid flux shear systems and implications for seismogenic processes, *Earth Planets Space* **54,** 1121–1125.

Di Luccio, F., A. Piscini, N. A. Pino, and G. Ventura (2005). Reactivation of deep faults beneath southern Apennines: Evidence from the 1990–1991 Potenza seismic sequences, *Terra Nova* **17,** 586–590, doi 10.1111/j.1365-3121.2005.00653.x.

Di Luccio, F., E. Fukuyama, and N. A. Pino (2005). The 2002 Molise earthquake: What can we learn about the tectonics of southern Italy?, *Tectonophysics* **405,** 141–154, doi 10.1016/j.tecto.2005.05.024.

Faulkner, D. R., T. M. Mitchell, D. Healy, and M. J. Heap (2006). Slip on 'weak' faults by the rotation of regional stress in the fracture damage zone, *Nature* **444,** 922–925, doi 10.1038/nature05353.

Frohlich, C., and S. D. Davis (1999). How well constrained are well-constrained *T*, *B* and *P* axes in moment tensor catalogs?, *J. Geophys. Res.* **104,** 4901–4910.

Hardebeck, J. L., and E. Hauksson (1999). Role of fluids in faulting inferred from stress field signatures, *Science* **285,** 236–239.

Hardebeck, J. L., and E. Hauksson (2001). Stress orientations obtained from earthquake focal mechanisms: What are appropriate uncertainty estimates?, *Bull. Seismol. Soc. Am.* **91,** 250–262.

Hollenstein, C., M. D. Müller, A. Geiger, and H.-G. Kahle (2008). Crustal motion and deformation in Greece from a decade of GPS measurements, 1993–2003, *Tectonophysics* **449,** 17–40, doi 10.1016/j.tecto.2007.12.006.

Kalogeras, I., D. Loukatos, and G. Stavrakakis (2008). Preliminary report of the strong motion data of the 8 June 2008 earthquake ($M_w$ 6.4) in Achaia–Elia, western Greece, http://www.gein.noa.gr/services/skyros.html.

Kamberis, E., S. Sotiropoulos, O. Aximniotou, S. Tsaila-Monopoli, and C. Ioakim (2000). Late Cenozoic deformation of the Gavrovo and Ionian zones in NW Peloponnese (western Greece), *Ann. di Geophys.* **43,** 905–919.

Kennedy, B. M., and M. C. van Soest (2007). Flow of mantle fluids through the ductile lower crust: Helium isotope trends, *Science* **318,** 1433–1436, doi 10.1126/science.1147537.

Kennedy, B. M., Y. K. Kharaka, W. C. Evans, A. Ellwood, D. J. DePaolo, J. Thordsen, G. Ambats, and R. H. Mariner (1997). Mantle fluids in the San Andreas fault system, California, *Science* **278,** 1278–1281.

Konstantinou, K. I., N. S. Melis, and K. Boukouras (2010). Routine regional moment tensor inversion for earthquakes in the Greek region: The National Observatory of Athens (NOA) database (2001–2006), *Seismol. Res. Lett.* **81,** 750–760, doi 10.1785/gssrl.81.5.750.

Konstantinou, K. I., N. S. Melis, S.-J. Lee, C. P. Evangelidis, and K. Boukouras (2009). Rupture process and aftershocks relocation of the 8 June 2008 $M_w$ 6.4 earthquake in northwest Peloponnese, Western Greece, *Bull. Seismol. Soc. Am.* **99,** 3374–3389, doi 10.1785/0120080301.

Laigle, M., A. Hirn, M. Sachpazi, and C. Clément (2002). Seismic coupling and structure of the Hellenic subduction zone in the Ionian islands region, *Earth Planet. Sci. Lett.* **200,** 243–253.

Melis, N. S., and G.-A. Tselentis (1998). 3-D *P*-wave velocity structure in western Greece determined from tomography using earthquake data recorded at the University of Patras seismic network (PATNET), *PAGEOPH* **152,** 329–348.

Michael, A. J. (1987). Use of focal mechanisms to determine stress: A control study, *J. Geophys. Res.* **92,** 357–368.

Michael, A. J. (1991). Spatial variations in stress within the 1987 Whittier Narrows, California, aftershock sequence: New techniques and results, *J. Geophys. Res.* **96,** 6303–6319.

Mittempergher, S., G. Pennacchioni, and G. Di Toro (2009). The effects of fault orientation on fault rock assemblages at seismogenic depths, *J. Struct. Geol.* **31,** 1511–1524, doi 10.1016/j.jsg.2009.09.003.

Morrow, C. A., D. E. Moore, and D. A. Lockner (2000). The effect of mineral bond strength and absorbed water on fault gouge frictional strength, *Geophys. Res. Lett.* **27,** 815–818.

Newell, D. L., L. J. Crossey, K. L. Karlstrom, T. P. Fischer, and D. R. Hilton (2005). Continental-scale links between the mantle and groundwater systems of the western United States: Evidence from travertine springs and regional He isotope data, *GSA Today* **15,** no. 12, 4–10.

Papazachos, B. C., and K. Papazachou (1997). *The Earthquakes of Greece*, Ziti editions, Thessaloniki.

Pik, R., and B. Marty (2009). Helium isotopic signature of modern and fossil fluids associated with the Corinth rift fault zone (Greece): Implication for fault connectivity in the lower crust, *Chemical Geol.* **266,** 67–75, doi 10.1016/j.chemgeo.2008.09.024.

Rice, J. R. (1992). Fault stress states, pore pressure distributions, and the weakness of the San Andreas Fault, in *Fault Mechanics and Transport Properties of Rocks*, B. Evans and T.-F. Wong (Editors), 475–505, Academic Press, San Diego, California.

Sachpazi, M., A. Hirn, C. Clément, F. Haslinger, M. Laigle, E. Kissling, P. Charvis, Y. Hello, J.-C. Lépine, M. Sapine, and J. Ansorge (2000). Western Hellenic subduction and Cephalonia transform: Local earthquakes and plate transport and strain, *Tectonophysics* **319,** 301–319.

Sibson, R. H. (1990). Rupture nucleation on unfavorably oriented faults, *Bull. Seismol. Soc. Am.* **80,** 1580–1604.

Sodoudi, F., R. Kind, D. Hatzfeld, K. Priestley, W. Hanka, K. Wylegalla, G. Stavrakakis, A. Vafidis, H.-P. Harjes, and M. Bohnhoff (2006). Lithospheric structure of the Aegean obtained from *P* and *S* receiver functions, *J. Geophys. Res.* **111,** B12307, doi 10.1029/2005JB003932.

Streit, J. (1999). Conditions for earthquake surface rupture along the San Andreas fault system, California, *J. Geophys. Res.* **104,** 17929–17939.

Streit, J., and S. F. Cox (2001). Fluid pressures at hypocenters of moderate to large earthquakes, *J. Geophys. Res.* **106,** 2235–2243.

Tembe, S., D. Lockner, and T.-F. Wong (2009). Constraints on the stress state of the San Andreas Fault with analysis based on core and cuttings from San Andreas Fault Observatory at Depth (SAFOD) drilling phases 1 and 2, *J. Geophys. Res.* **114,** B11401, doi 10.1029/2008JB005883.

Tenthorey, E., and S. F. Cox (2006). Cohesive strengthening of fault zones during the interseismic period: An experimental study, *J. Geophys. Res.* **111,** B09202, doi 10.1029/2005JB004122.

Institute of Geophysics
National Central University
Jhongli, 320 Taiwan
kkonst@ncu.edu.tw
(K.I.K.)

Institute of Geodynamics
National Observatory of Athens
POB 20048
11810 Athens, Greece
(C.P.E., N.S.M.)

Manuscript received 24 March 2010